UVSQ université PARIS-SACLAY
Observatoire de Versailles Saint-Quentin-en-Yvelines
CAMPUS DE SAINT-QUENTIN-EN-YVELINES
cnrs
SORBONNE UNIVERSITÉ
CRÉATEURS DE FUTURS DEPUIS 1257

No evidence of solar oblateness variations correlated with solar activity during cycles 24 and 25

PNST – January 2024, Marseille

Mustapha Meftah

LATMOS
cnrs

1 – Introduction

❑ First objective

- **Perform an in-depth analysis of the complete solar disk images obtained by the SDO/HMI instrument over an entire solar cycle (spanning from February 2010 to today), aiming to achieve the most accurate measurements of solar oblateness ($\Delta_\odot = \Delta R/R$) and the Sun's gravitational moments (Jn), based on solar limb shape.**
- **Determine the solar gravitational moments using the differential rotation profiles of the Sun from SoHO/MDI & SDO/HMI data, covering a period from May 1996 to the present.**
- **Refute or confirm the variability of the solar shape with the solar cycle activity and analyze its correlation with the spectral irradiance in the observed wavelength range.**

  → Knowing the temporal solar shape changes is important since the oblateness is sensitive to the interior rotation and mass distribution and other photospheric stresses.
  → A variable solar shape requires either enigmatically large perturbation of the interior mass/rotation distribution, or it implies a confusion in the measured solar shape caused by, for example, photospheric magnetic contamination.

❑ Second objective

- **Refine observations of a large solar rotation shear in the extreme outer photosphere.**

  → A better understanding of the photospheric shear could be important for explaining the rotation gradient below the photosphere in the outer 5% of the convection zone.

1 – Introduction

❑ Scientific impacts

- **Solar oblateness is a diagnostic of the internal rotation. Because the Sun is not a solid body, both gravitational and rotational effects cause a very slight flattening.**
  - ✓ **The lowest-order term of solar flattening is linked to the quadrupole moment, denoted as J2. It represents a crucial parameter for understanding the Sun's shape, its internal dynamics, and its influence on the solar system.**
  - ✓ **The next highest term, J4, is sometimes called octopole and sometimes hexadecapole. It represents a more complex asphericities in the Sun's shape and provides information about the Sun's magnetic field structure and its variation over the solar cycle. This is because the magnetic field can influence the distribution of mass and, consequently, the Sun's gravitational field.**
- **It represents a validation of the physical hypotheses implemented in the solar models.**
- **It provides valuable insights into the rotation of the Sun's inner layers and subsurface magnetism (internal rotation generating the magnetism that creates solar variability).**
- **The exact shape of the Sun allows for one of the tests of Albert Einstein's General Relativity (the precise distribution of solar mass determines how the Sun affects the orbit of all planets, particularly that of Mercury). Accurate calculation of planetary ephemerides. In the formalism of the parameterized post-Newtonian relativistic theory (known as PPN), the prediction of the advance of Mercury's perihelion per orbital period is related to the parameter λp, itself directly linked to the solar quadrupole moment J2.**

1 – Introduction

❑ Instrumentation used to conduct the analyses

- **Michelson Doppler Imager (MDI) on the Solar and Heliospheric Observatory (SoHO)**

MDI operates at a wavelength of 676.8 nm with a resolution of 1.4 arc-seconds, targeting the nickel (Ni I) solar spectral line. This narrow wavelength band is chosen specifically for its sensitivity to the Doppler shifts caused by solar surface motions and magnetic fields. The data taken by MDI covers the time from 1996 until April 2011.

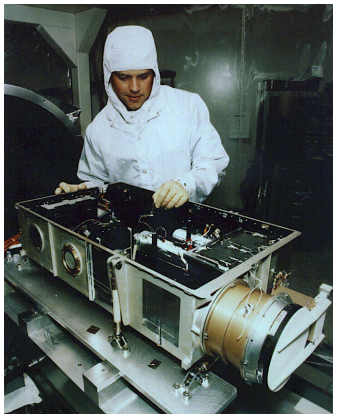

- **Helioseismic and Magnetic Imager (HMI) on the Solar Dynamics Observatory (SDO)**

HMI operates at a wavelength of 617.3 nm (1 arc-second resolution), which corresponds to a Fe I absorption line. HMI is designed to study oscillations and the magnetic field at the solar surface, or photosphere.
HMI is making accurate measurements of the solar shape since 2010 and covers a full solar cycle. The solar oblateness measurements are performed every six months during a calibration maneuver where the SDO spacecraft is rotated 360 degrees in 32 steps around the spacecraft to Sun line.

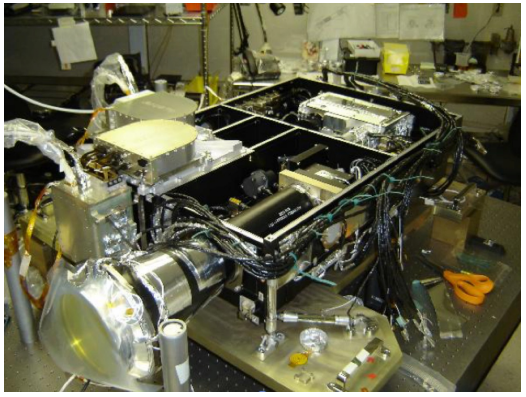

1 – Introduction

❑ Additional dataset used

- **Sunspot Number and Sunspot Area Butterfly Diagram**

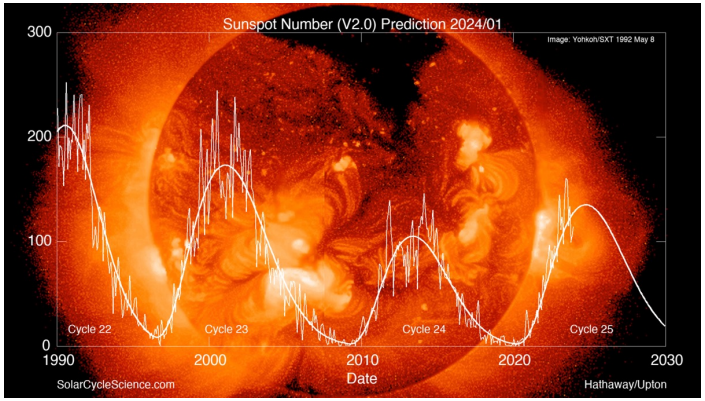

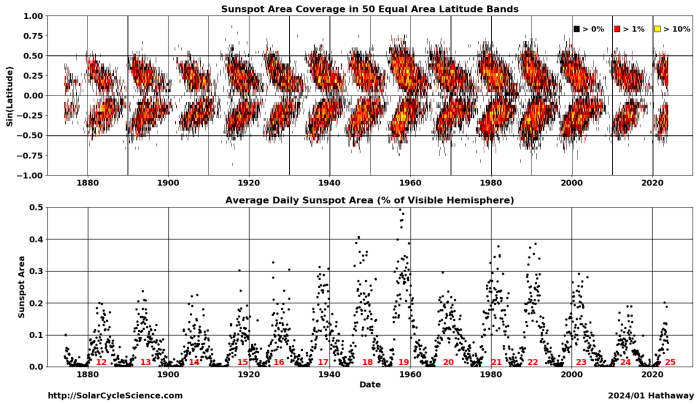

- **Solar spectrum**

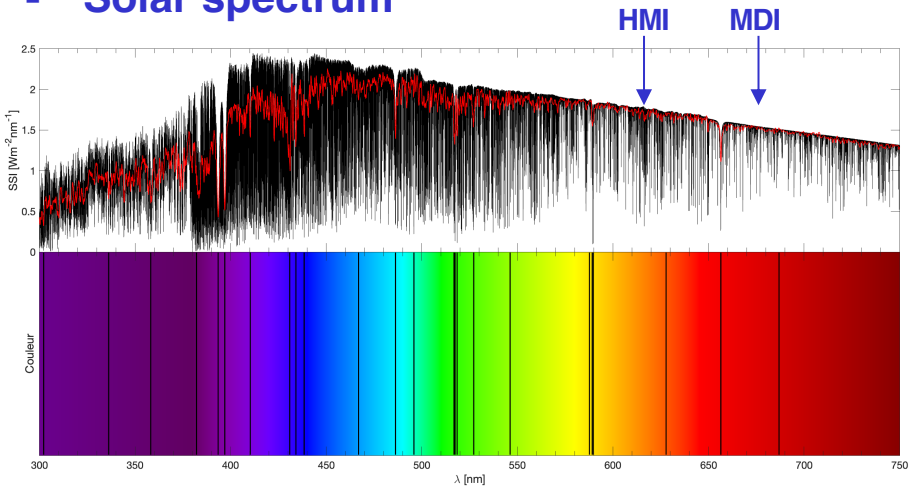

Data set name	Data type	Wavelength coverage	Spectral resolution	Sampling
SOLAR-HRS Disk-integrated spectrum	Composite Solar spectral irradiance	0.5 – 4399.1 nm	SOLAR-ISS (< 300 nm): < 1.0 nm QASUMEFTS (300 – 380 nm): < 0.025 nm SPTS (> 380 nm): <0.01 nm	< 0.02 nm
SOLAR-HRS Disk-center (μ = 1.0)	Composite Solar spectral irradiance	650.0 – 4399.1 nm	SPTS: < 0.01 nm	< 0.02 nm
SOLAR-HRS Intermediate cases Solar positions μ = 1.0, 0.9, 0.8, 0.7, 0.6, 0.5, 0.4, 0.3, 0.2, 0.1, 0.05	Composite Solar spectral irradiance	650.0 – 4399.1 nm	SPTS: < 0.01 nm	< 0.02 nm
SOLAR-HRS AM1.5 Disk-Integrated Spectrum	Composite Solar spectral irradiance	0.5 – 4399.1 nm	SOLAR-ISS (< 300 nm): < 0.1 nm QASUMEFTS (300 – 380 nm): < 0.025 nm SPTS (> 380 nm): < 0.01 nm	< 0.02 nm
SOLAR-HRS AM1.5 (air) Disk-Integrated Spectrum	Composite Solar spectral irradiance	0.5 – 4399.1 nm	SOLAR-ISS (< 300 nm): < 0.1 nm QASUMEFTS (300 – 380 nm): < 0.025 nm SPTS (> 380 nm): < 0.01 nm	< 0.02 nm
MPS-ATLAS-Kurucz Disk-Integrated Spectrum	Solar Model	250.0 – 5000.0 nm	< 0.01 nm	< 0.01 nm
MPS-ATLAS-Kurucz Disk-center (μ = 1.0)	Solar Model	250.0 – 5000.0 nm	< 0.01 nm	< 0.01 nm
MPS-ATLAS-Vald3 Disk-Integrated Spectrum	Solar Model	250.0 – 5000.0 nm	< 0.01 nm	< 0.01 nm
MPS-ATLAS-Vald3 Disk-center (μ = 1.0)	Solar Model	250.0 – 5000.0 nm	< 0.01 nm	< 0.01 nm

http://doi.latmos.ipsl.fr/DOI_SOLAR_HRS.v1.1.html

Meftah et al., 2023

The solar reference spectra used in this work are available at: https://cdsarc.cds.unistra.fr/viz-bin/cat/VI/159.

2 – Methods

❑ Determination from helioseismology and from limb shape observations

- **A) Solar gravitational moments J2n using helioseismic inference of internal rotation (MDI and HMI) and theoretical solar oblateness estimation.**

$$\phi_{out}(r,u) = -\frac{GM_\odot}{r}\left[1 - \sum_{n=1}^{\infty}\left(\frac{R_\odot}{r}\right)^{2n} J_{2n}P_{2n}(u)\right]$$

$$J_{2n} = -\left[\frac{x^{2n}}{(2n+1)\psi_{2n} + x\psi'_{2n}}\right]_{x=1} \times \int_0^1 \left(\left(x^2(U-4)U\psi_{2n} - x^3U\psi'_{2n}\right)A_{2n} + x^2U\psi_{2n}B_{2n}\right)\mathrm{d}x$$

- **B) Solar oblateness ($\Delta_\odot$ = ΔR/R) determination from HMI solar limb shape.**

$$r(\theta) = <r>\left[1 + \sum_{n=1}^{\infty} C_{2n}P_{2n}(\cos(\theta))\right] = <r>\left[1 + C_2P_2(\cos(\theta)) + C_4P_4(\cos(\theta)) + \ldots\right]$$

$$\Delta r_\odot = r\left(\frac{\pi}{2}\right) - r(0) = <r> \times \left(-\frac{3}{2}C_2 - \frac{5}{8}C_4\right) \simeq R_\odot \times \left(-\frac{3}{2}C_2 - \frac{5}{8}C_4\right)$$

$$\Delta_\odot = -\frac{3}{2}C_2 - \frac{5}{8}C_4$$

$$\Delta_\odot = \frac{R_{eq} - R_{pol}}{R_{eq}} = \frac{\Delta r_\odot}{R_{eq}}$$

$\Delta_\odot \approx (3/2)\ J2 + (\delta r/R)$, where $\delta r/R = 8.1\ 10^{-6}$ (Dicke 1970)

2 – Methods

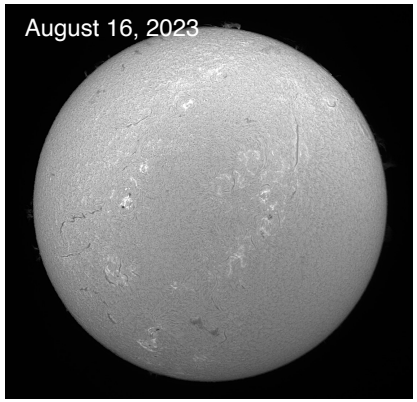

656.3 nm (H-alpha)

❑ Solar oblateness determination from HMI solar limb shape

- **Solar radius determination (Rij) for N images at all θ**
- **Mean solar radius evolution (<R>) and brightness (<B>)**

$$\langle R \rangle = \frac{1}{N \times N_\theta} \sum_{m=1}^{N} \sum_{n=1}^{N_\theta} R_{(m,n)} \qquad \langle B \rangle = \frac{1}{N \times N_\theta} \sum_{m=1}^{N} \sum_{n=1}^{N_\theta} B_{(m,n)}$$

- **Image distortion determination**

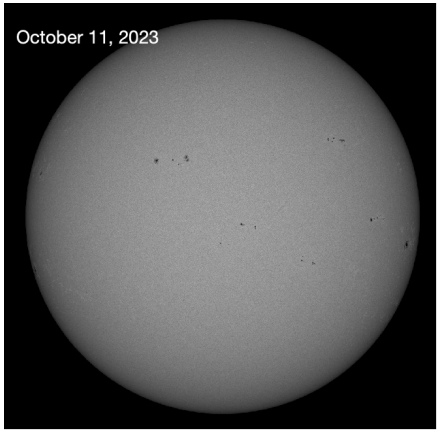

617.3 nm (Fe I)

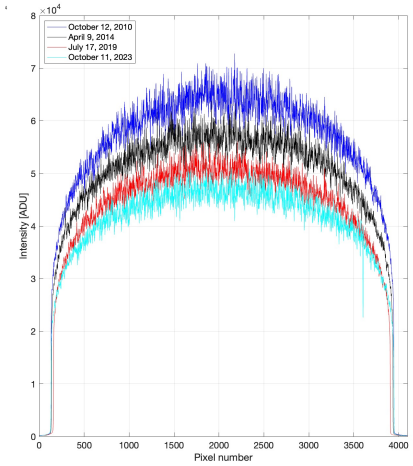

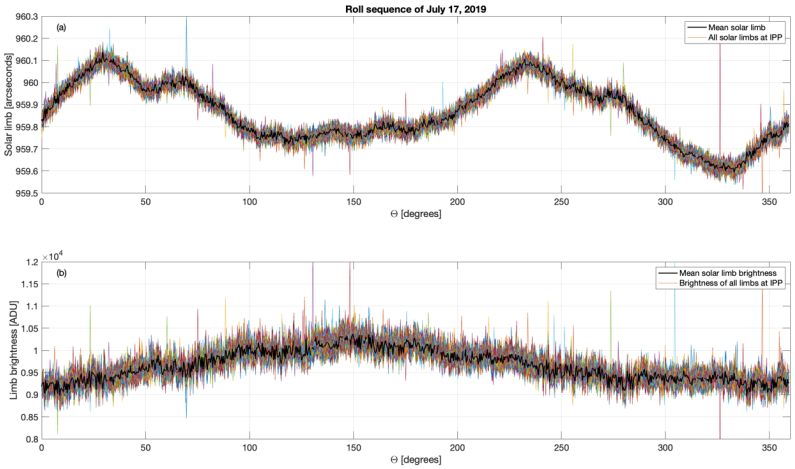

- **Data correction (M1 and M2 methods)**

M1 method:

$$Rc_{(i,j)} = R_{(i,j)} + \langle R \rangle - \frac{1}{N_\theta} \sum_{n=1}^{N_\theta} R_{(i,n)}$$

M2 method:

$$Rb_{(i,j)} = Rc_{(i,j)} + \alpha \frac{B_{(i,j)} - \langle B \rangle}{\frac{dB}{dR(i,j)}}$$

- **Apparent solar oblateness determination (Legendre polynomials)**
- **Heliographic latitude correction (correction for the tilt of the ecliptic → B0 angle)**

3 – Results

❑ Gravitational moments determination using CESAM and ASTEC solar models

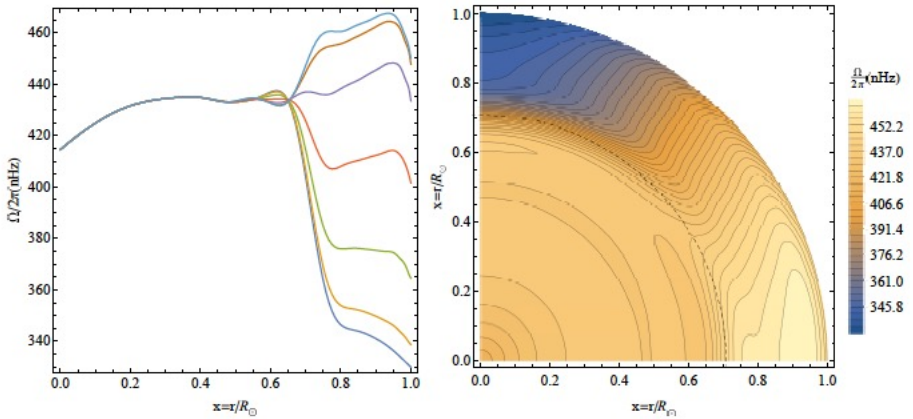

Figure 1. Time-averaged rotation profiles $\Omega/2\pi$ obtained from RLS inversion of HMI data collected between April 2010 and July 2020. Left panel: Radial profiles given each 15° from equator (top) to pole (bottom). Right Panel: Contours of iso-rotation.

CESAM (Code d'Évolution Stellaire Adaptatif et Modulaire) and ASTEC (Aarhus Stellar Evolution Code) are designed to provide detailed and accurate models of stellar structure, particularly for stars like the Sun.

Rotation data	Solar model	$J_2(\times10^{-7})$	$J_4(\times10^{-9})$	$J_6(\times10^{-10})$	$J_8(\times10^{-11})$	$J_{10}(\times10^{-12})$
SDO/HMI	CESAM	2.211	-4.252	-1.282	5.897	-4.372
	ASTEC	2.216	-4.256	-1.283	5.901	-4.375
SoHO/MDI	CESAM	2.204	-4.064	-1.136	5.404	-3.993
	ASTEC	2.208	-4.069	-1.137	5.408	-3.996

3 – Results

- **J2n and solar oblateness determination using helioseismic inference of internal rotation**

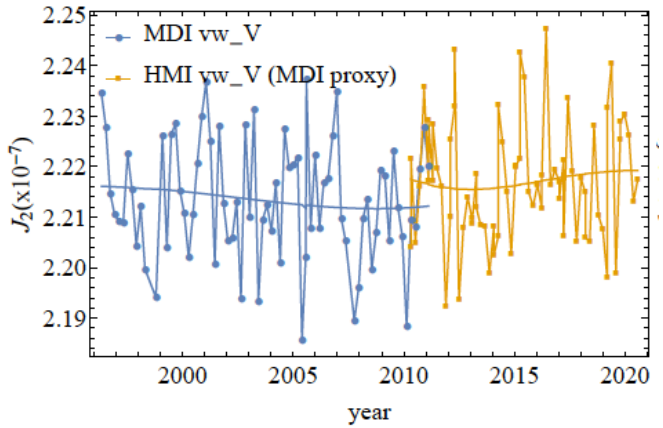

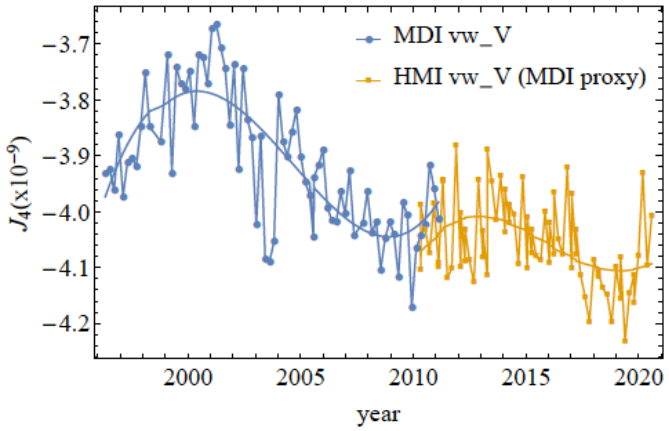

Solar structure is considered using a model obtained from CESAM stellar evolution code.

The precise theoretical calculation of surface density distortion coefficients D2n of the Sun (vs. *its observational counterpart C2n obtained from the analysis of space based solar limb shape measurements*) is very important to interpret observed solar limb fluctuations, which reflect physical mechanisms inside the Sun.

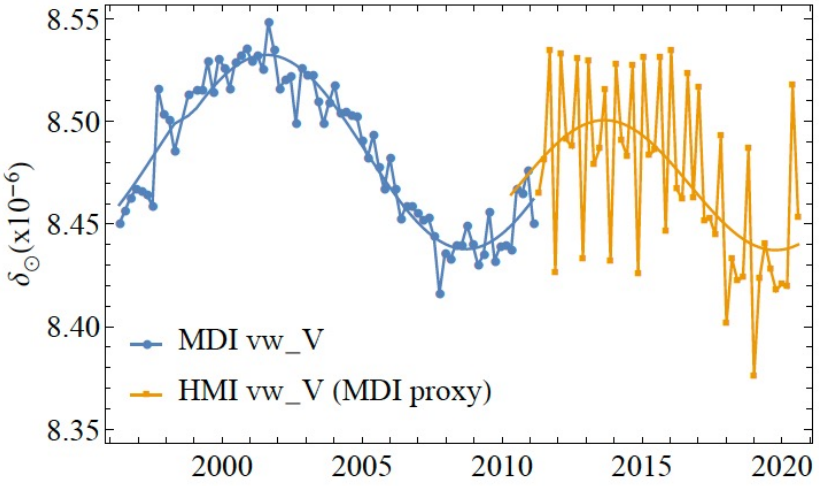

Mecheri and Meftah, 2024

3 – Results

❑ Solar oblateness determination from HMI solar limb shape

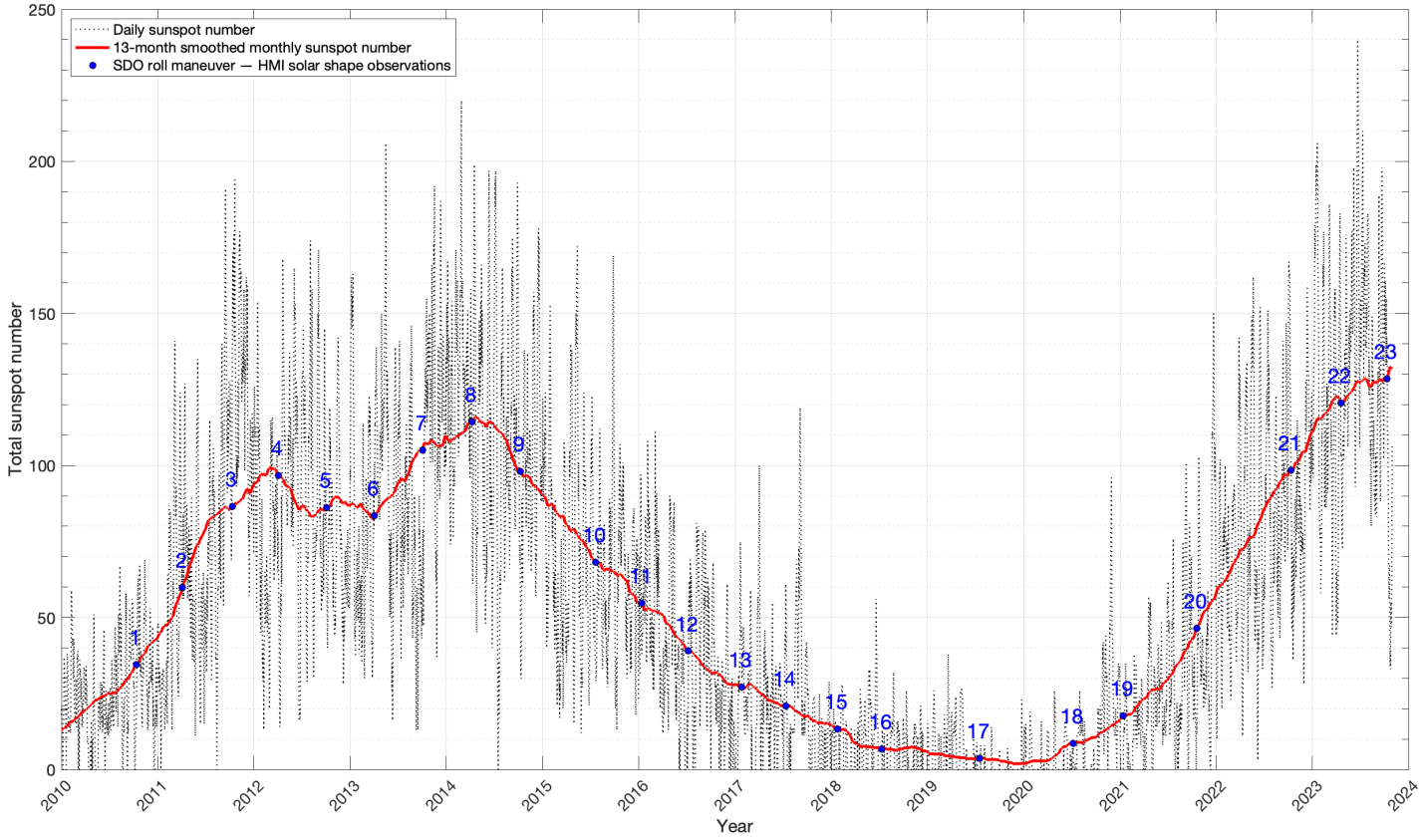

The SDO roll maneuver is essential to determining the solar shape in order to remove instrument optical distortion. The 23 roll maneuvers have been performed at 6 month intervals (typically April and October). The spring and fall roll maneuvers have the spacecraft rotate in opposite directions.

The HMI observing sequence takes continuum tuned and line core images with one camera in 2 circular and 4 linear polarizations for the primary solar shape determination.

3 – Results

❑ Solar oblateness determination from HMI solar limb shape

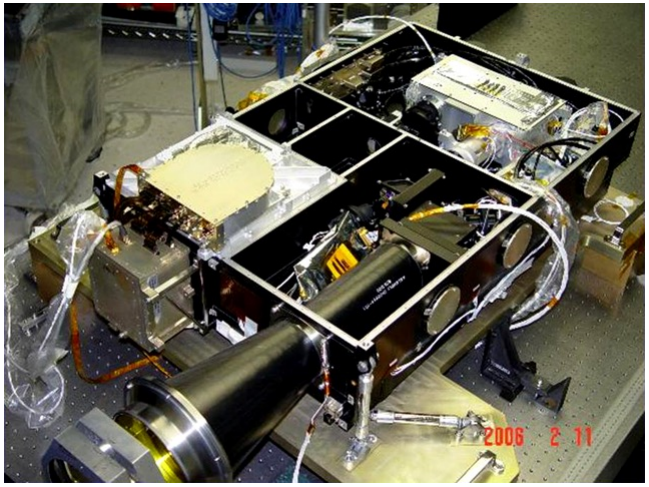

FID	PL index	Polarization state
Standard observing-program FIDs		
10**0	410	Mod A pol 1
10**1	411	Mod A pol 2
10**2	412	Mod A pol 3
10**3	413	Mod A pol 4
10**4	414	$I+Q$; linear polarization, 0 deg
10**5	415	$I-Q$; linear polarization, 90 deg
10**6	416	$I+U$; linear polarization, 45 deg
10**7	417	$I-U$; linear polarization, 135 deg
10**8	418	$I+V$; left circular polarization
10**9	419	$I-V$; right circular polarization

- **Magnetic Field Mapping:** One of the primary uses of polarimetry in solar physics is to study the Sun's magnetic field. The polarization of light from the Sun can be affected by the magnetic field through the Zeeman effect. By measuring the polarization states (Stokes I, Q, U, and V), we can infer the strength and direction of magnetic fields in the solar atmosphere.
- **Studying Solar Flares and Active Regions:** Polarization measurements help in understanding the complex processes in solar flares and active regions. These regions exhibit strong magnetic fields that can influence the polarization of emitted light. Analyzing these polarizations allows to gain insights into the physics of these high-energy events.
- **Solar Atmosphere Dynamics:** Different layers of the solar atmosphere can be studied using polarimetry. For instance, the chromosphere and corona have distinct polarization signatures. Polarimetric studies can help understand the dynamics, temperature, and compositions of these layers.

3 – Results

❑ Solar oblateness determination from HMI solar limb shape

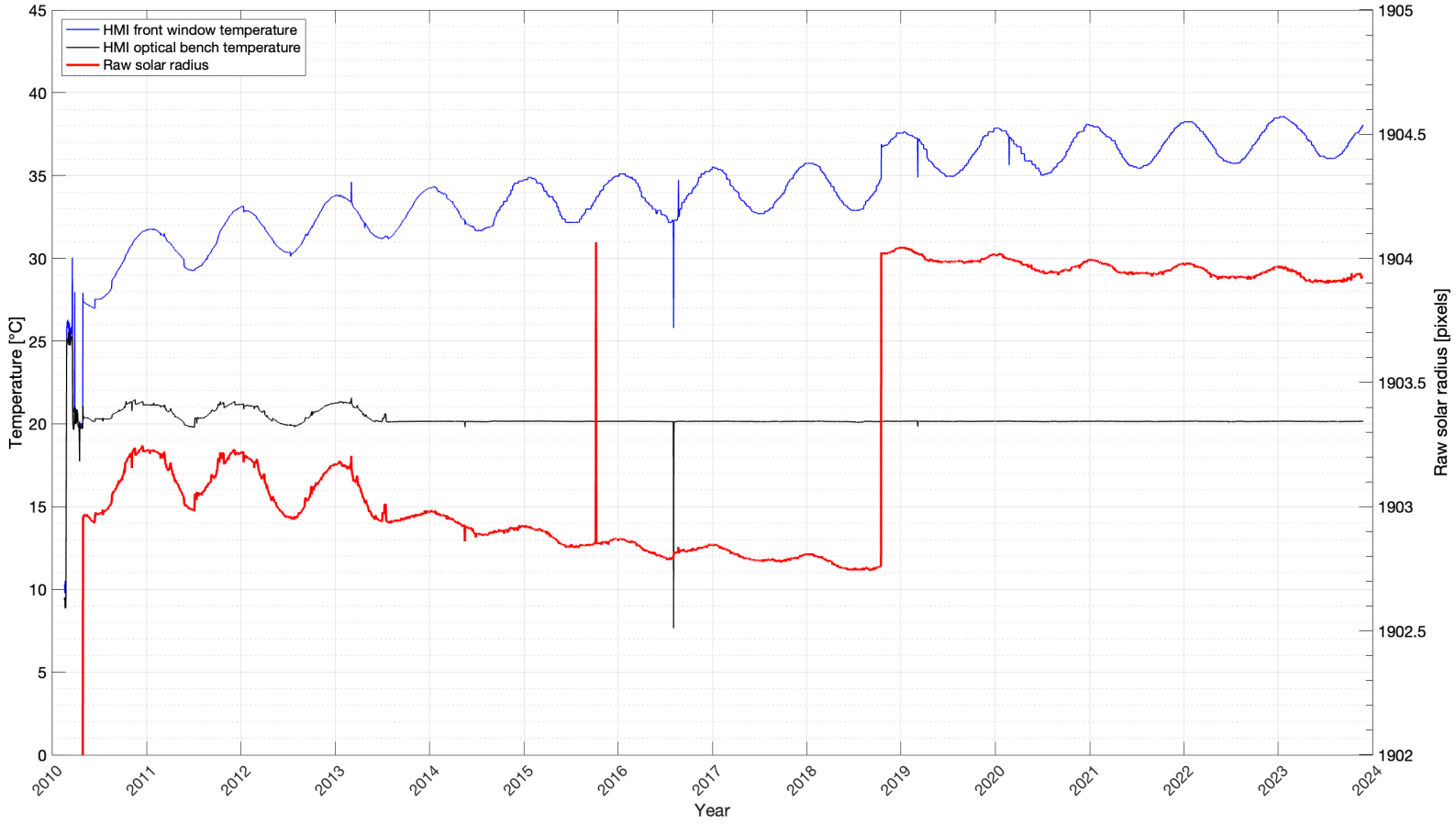

The HMI optical bench temperatures show an annual variation because the initial thermal control scheme ran the heaters at a constant duty cycle. The thermal control scheme has been modified in 2013 to adjust the heater duty cycles to maintain a more uniform temperature of 20 degrees C.

3 – Results

❑ Solar oblateness determination from HMI solar limb shape

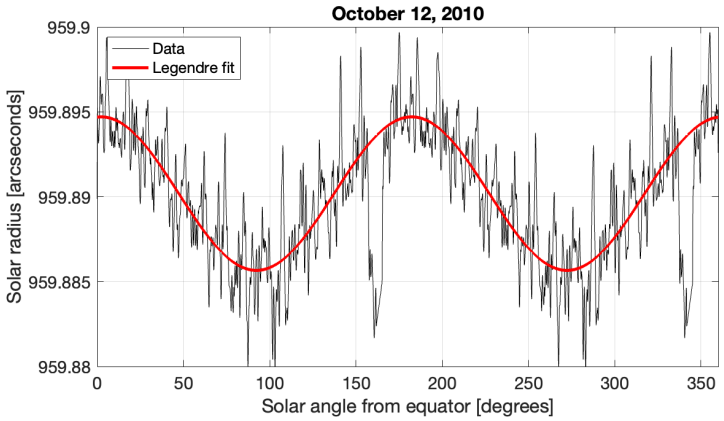

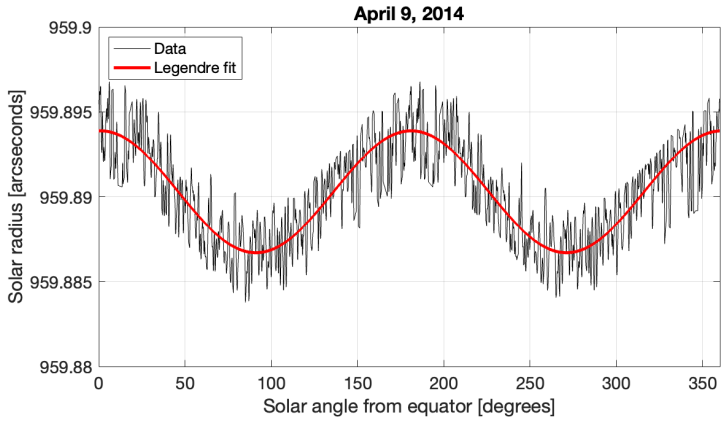

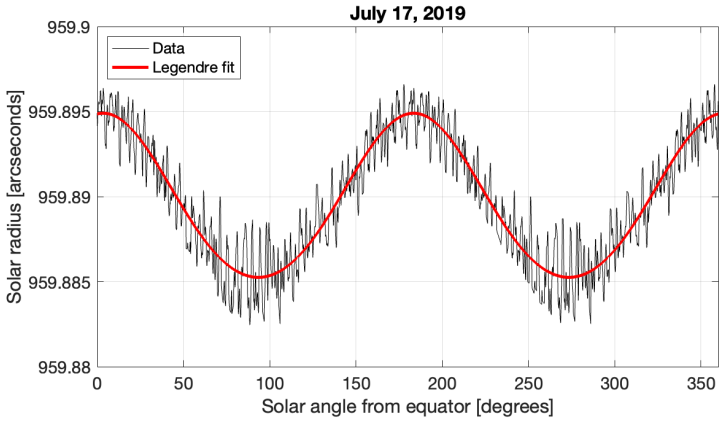

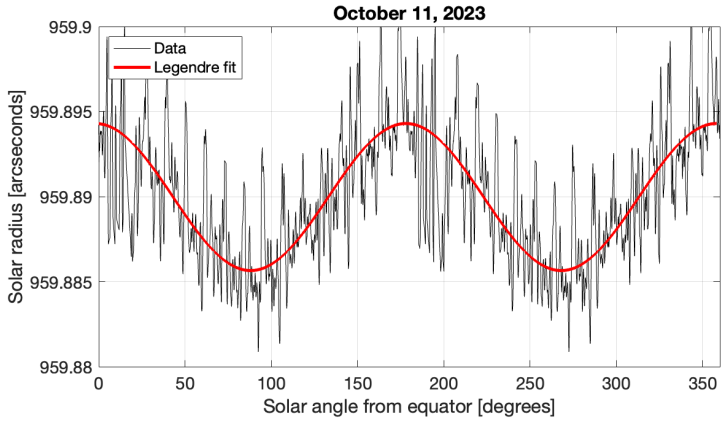

Solar Oblateness is caused by two main factors: firstly, by the deformation induced by centrifugal force on the surface layers, which is proportional to the square of the angular rotation, and secondly, by the alteration of the gravitational potential due to the distortion of the Sun's interior, also as a result of the centrifugal force.

3 – Results

❑ Solar oblateness determination from HMI solar limb shape

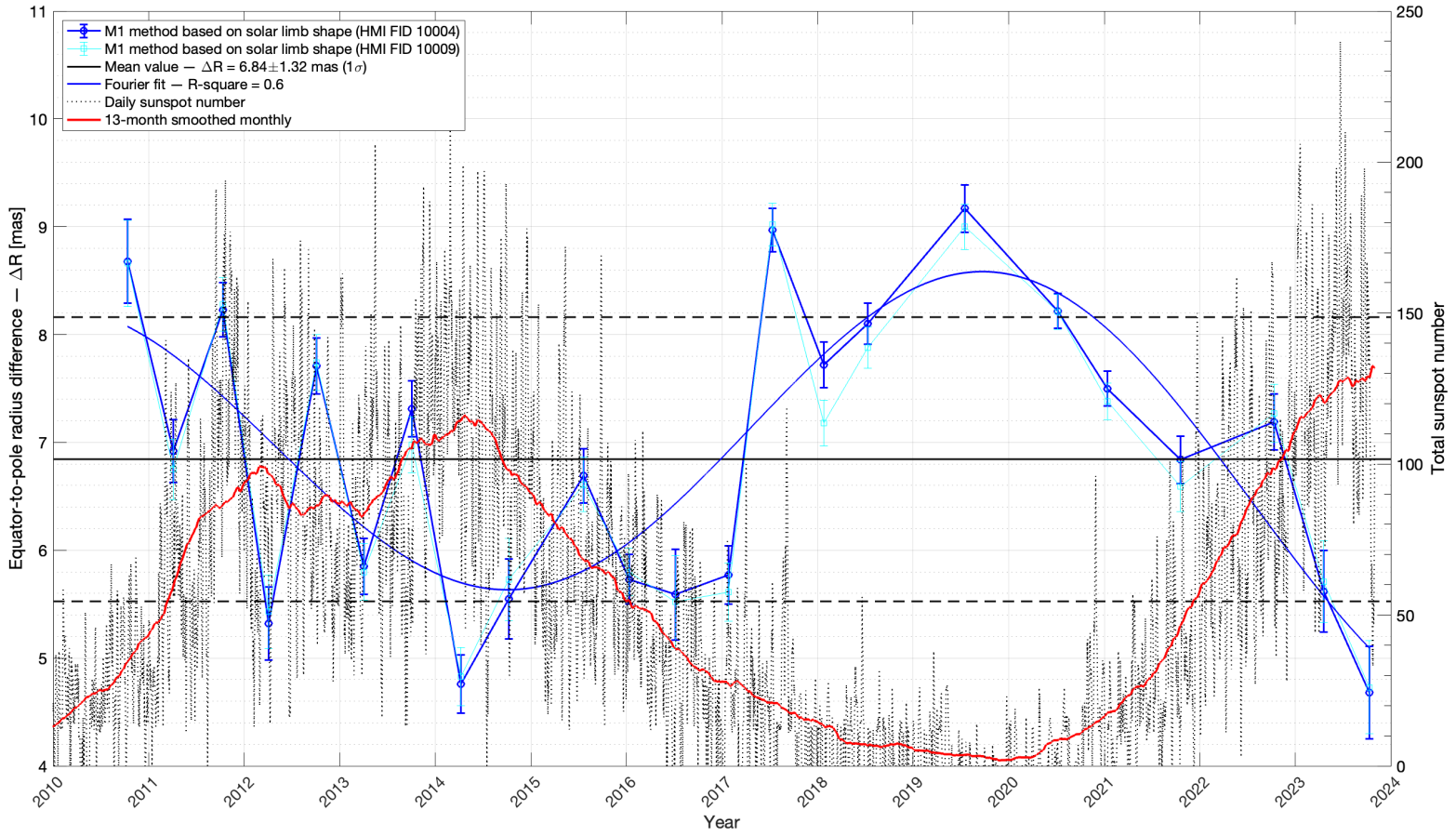

3 – Results

❑ Solar oblateness determination from HMI solar limb shape

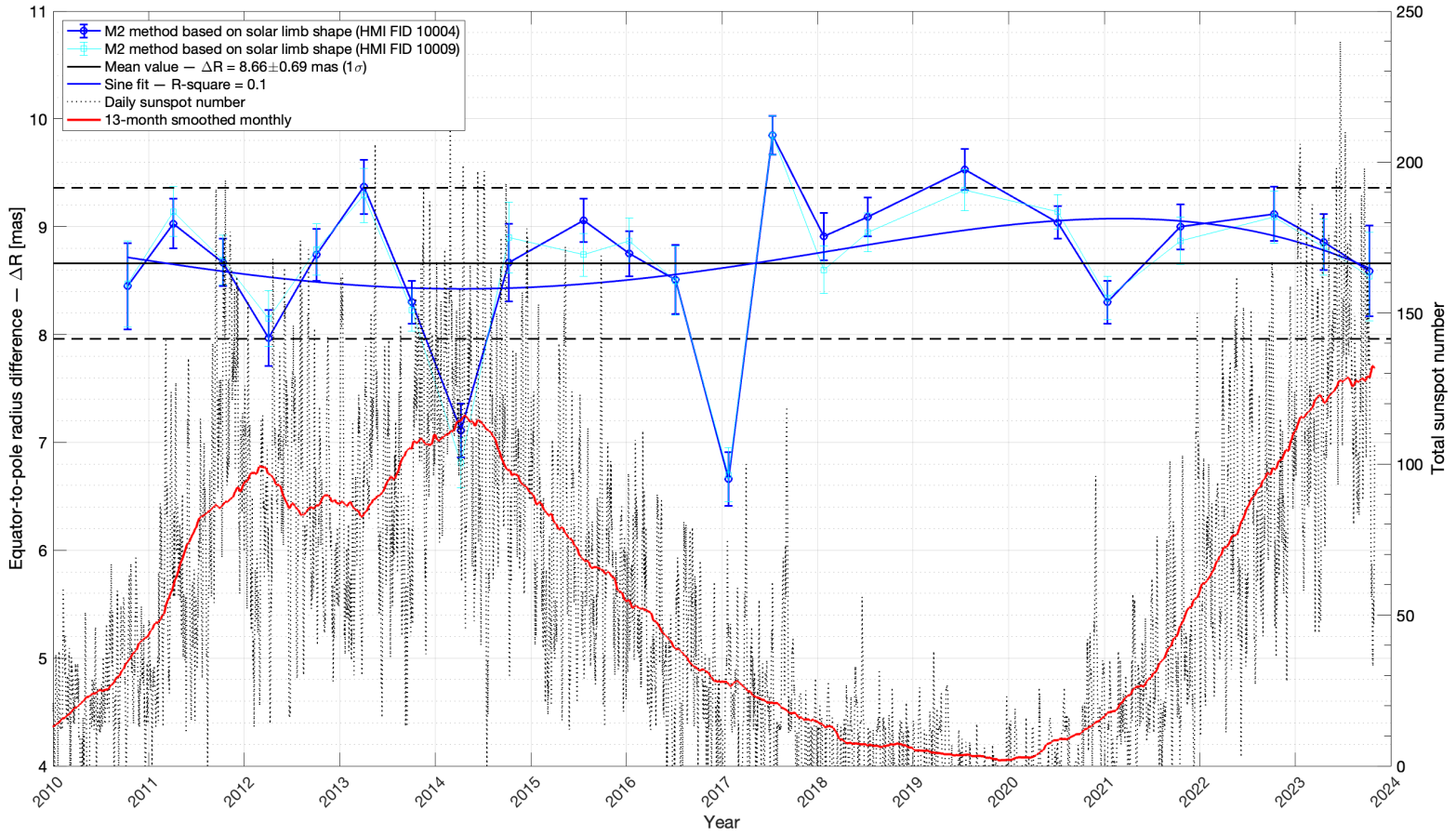

3 – Results

❑ Solar oblateness determination from HMI solar limb shape

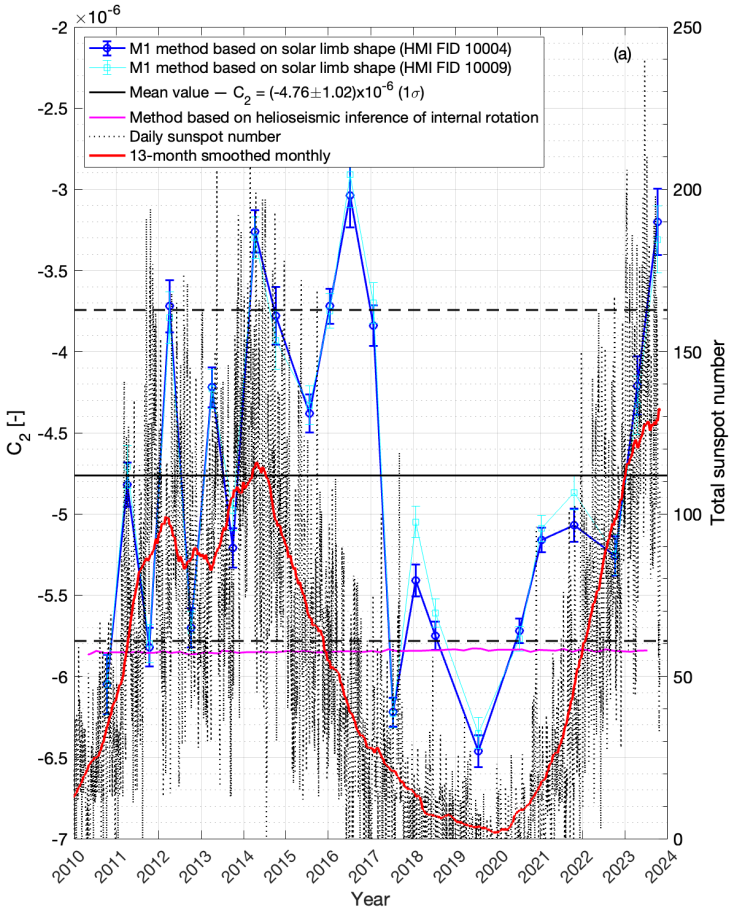

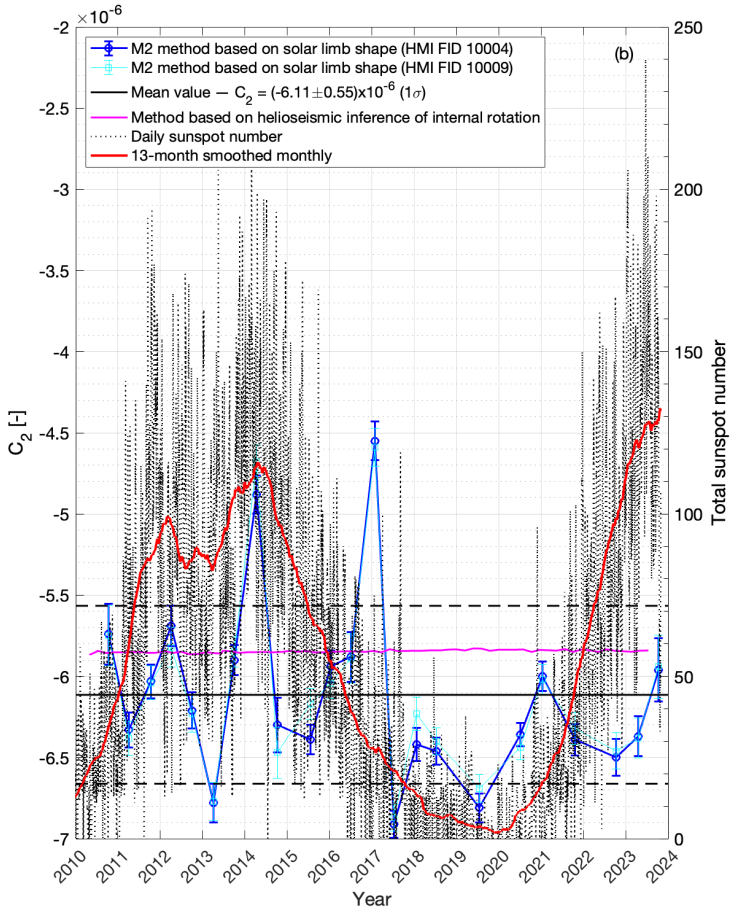

3 – Results

❑ Solar oblateness determination from HMI solar limb shape

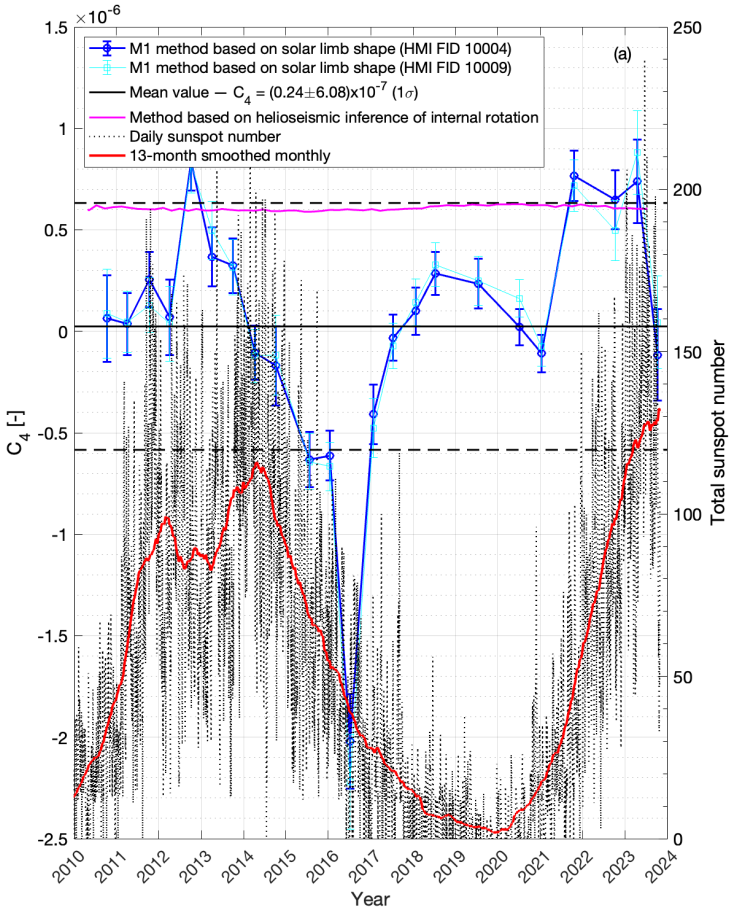

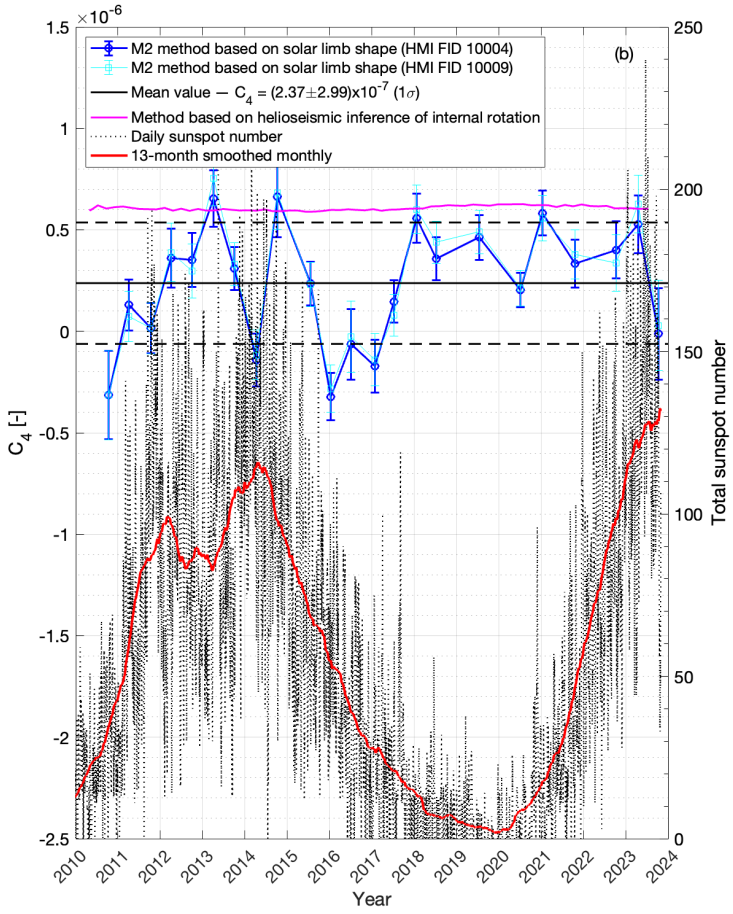

3 – Results

❑ Solar oblateness determination from HMI solar limb shape

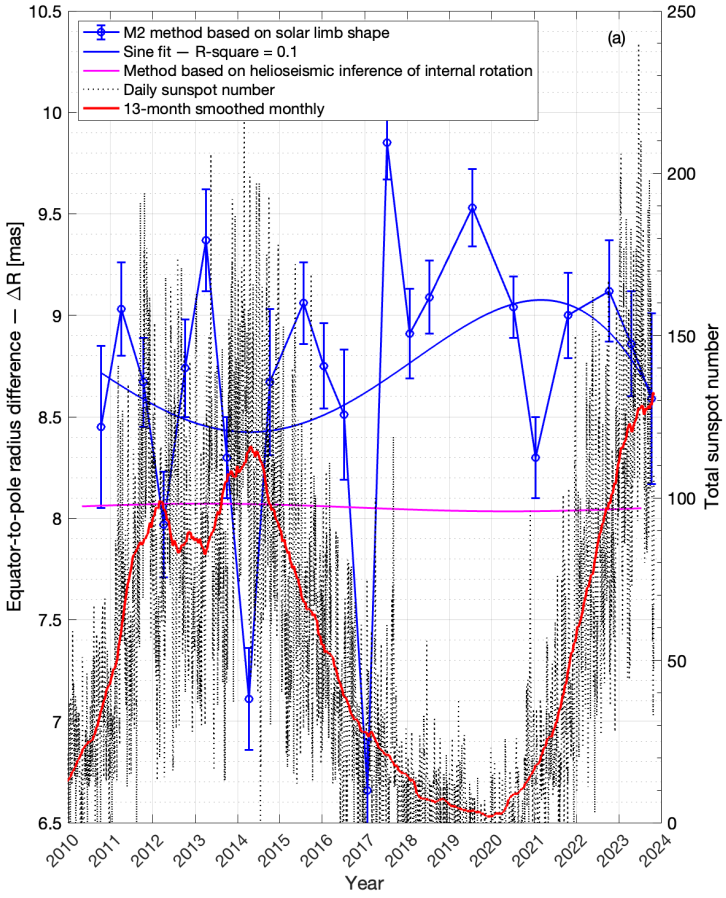

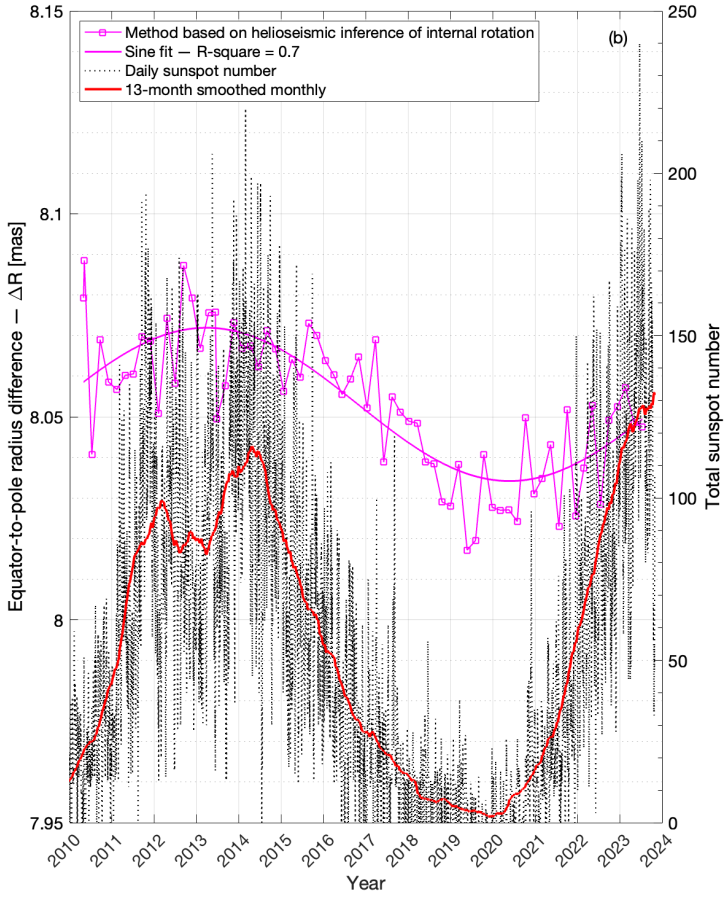

Meftah and Mecheri, 2024

Conclusions

Solar oblateness was determined using two methods (helioseismic inference of internal rotation and solar limb shape observations) and results obtained are consistent. The average solar equator-to-pole radius difference obtained is 8.05±0.14 mas at 1σ for the first approach, and 8.66±0.69 mas at 1σ for the second approach.

23 roll calibration maneuvers have been performed with success during the SDO mission to date. The analysis of the theoretical solar oblateness obtained using continuous internal rotation rates inferred from helioseismic data of HMI and HMI limb shape indicates that the solar oblateness has stayed roughly constant over the 14 years of observation.

We note that the solar oblateness determined from helioseismology shows a slight variation in phase with solar activity. Conversely, the solar oblateness determined from the solar limb shape seems to be in anti-phase with solar activity. However, there is no evidence of temporal variability in the Sun's shape and no evidence that these solar oblateness measurements were temporally affected by near-surface (or dynamo/interior) magnetic fields.

A variable solar shape requires either enigmatically large perturbation of the interior mass/rotation distribution, or it implies a confusion in the measured solar shape caused by, for example, photospheric magnetic contamination.

Conclusions

The physical interpretation of the obtained results regarding solar oblateness, especially the observed discrepancies between measurements helioseismology and those provided solar disk, needs to be connected to the theoretical outcomes we achieve.

Helioseismology reveals that the disturbances in the Sun's spherical symmetry are localized in its outer layers (subsurface layers). These surface disturbances are closely correlated with solar activity.

However, a limitation of helioseismology is that it can probe the Sun's interior only up to a maximum surface radius of ~ 0.96R, which is significantly below the 1.00R surface where we calculate the D2n coefficients. This limit is set by the nature of the acoustic waves used in helioseismology, which can penetrate to a certain depth before being refracted back to the surface.

Regarding the solar disk measurements, we believe they also extend beyond 0.96R. The divergence between results might stem from analyzing at different radii. These behavioral differences have been previously discussed by Emilio (2007) and Lefebvre (2006, 2007), suggesting non-homologous expansion of the Sun's internal layers. This was further confirmed by numerical simulations conducted by Sofia (2005).

On the other hand, asphericities are caused by rotation and possibly by the presence of an internal magnetic field or any other factor that could break the Sun's spherical symmetry.

Therefore, helioseismology accounts for all these effects when calculating asphericities.

The question arises: Is this also true for solar limb measurements?